

# Experimental and Computational Investigations on Strain Rate Sensitivity and Deformation Behavior of Bulk Materials Made of Epoxy Resin Structural Adhesive

Takeshi Iwamoto\*+, Toshimasa Nagai\*\*, Toshiyuki Sawa\*

\* Graduate School of Engineering, Hiroshima University, Japan

\*\* Kobe Shipyard and Machinery Works, Mitsubishi Heavy Industries, Ltd., Japan

## Abstract

The deformation behavior and strain rate sensitivity of an epoxy resin structural adhesive and a CTBN (carboxyl-terminated butadiene-acrylonitrile) - modified epoxy resin adhesive are experimentally investigated using an INSTRON-type material testing machine and a split Hopkinson pressure bar apparatus. The experimental results show some fundamental features of a typical compressive stress-strain behavior of amorphous glassy polymers with linear elastic and nonlinear inelastic deformation stages. In the inelastic deformation, a peak stress and a strain-softening stage after the peak can be observed in the entire range of strain rate from  $10^{-4}$  to  $10^3$  s<sup>-1</sup>. In addition, it can be found that the relationship between the peak stress and strain rate on a semi-logarithmic plot is linear in the range of low strain rate. However, the slope of the curve changes at a high strain rate, and the nonlinear behavior of the peak stress can be obtained against the strain rate. In order to describe such a nonlinear peak stress - strain rate relationship and the deformation behavior of the structural adhesives in a wide range of strain rate on the basis of the experimental results, a plastic shear strain rate is formulated. Then, a three - dimensional constitutive model is derived based on a four - elements model with an elastic series element by considering the adhesive to be a glassy polymer. The plastic deformation rate tensor is expressed by the effective stress, which is the difference between the total stress and back stress, and the plastic shear strain rate proposed here. The stress tensor can be obtained by solving nonlinear

simultaneous equation. The formulated constitutive model is implemented into the commercial FE code, ABAQUS/Explicit, and then a computational simulation is performed. As a result, the validity of the proposed model is shown by comparing the experimental result.

**Key Words:** Structural Adhesive, Impact Deformation Behavior, Constitutive Equation, Split Hopkinson Pressure Bar, Finite Element Method

Abbreviated title: Strain Rate Sensitivity of Bulk Epoxy Resin Structural Adhesive

+Postal address: 1-4-1 Kagamiyama, Higashi-Hiroshima, Hiroshima, 739 - 8527 Japan

Tel: +81-824-24-7576, Fax.: +81-824-22-7193

E-mail: [iwamoto@mec.hiroshima-u.ac.jp](mailto:iwamoto@mec.hiroshima-u.ac.jp)

## 1. INTRODUCTION

With the development of polymer science in recent years, the use of adhesive bonding has been expanding in mechanical structures and electronic devices (Fay, 2005). In accordance with a demand for these usages, it is very important to increase its performance against deformation and their adhesive strength. To improve the performance, fundamental research work based on polymer science and engineering is necessary, as well as applied research work such as the evaluation of adhesive joint strength (Yokoyama and Shimizu, 1998; Sato and Ikegami, 1999, 2001).

In automobiles and other transportation industries, the use of adhesive bonding for important parts is being actively considered to decrease carbon emission and to realize a lightweight structure. In such a case, a detailed study of the stress distribution in such adhesive joints under impact loading is essential since the adhesive joints undergo impact loading (Yokoyama and Shimizu, 1998; Sato and Ikegami, 1999, 2001). In an adhesive joint, there are three fracture modes namely the interfacial fracture from the interface between an adhesive and adherend, the cohesive fracture in the adhesive and a mixed fracture as a combination of these fractures. There are many reports that the mixed fracture mode is dominant under an impact load (Yokoyama and Shimizu, 1998; Sato and Ikegami, 1999) and an evaluation of the deformation behavior of its bulk materials, which becomes part of the fracture behavior in the adhesive joint, will be crucial. Consequently, there have been some research works on the deformation behavior of bulk adhesive material (Yu et al., 2001; Goglio et al., 2008), but it is difficult to conclude whether the elasto-viscoplastic deformation behavior of the polymers was sufficiently considered.

The adhesive after solidification is a polymeric material such as a polycarbonate (PC) and poly methyl methacrylate (PMMA). For amorphous polymers other than the adhesives, a variety of fundamental studies can be found, such as on the rapid increase of yield stress at very high strain rate and it has been known to show a nonlinear behavior against increasing strain rate (Mulliken and Boyce, 2006; Nishida et al., 2009). This is believed to be due to a secondary relaxation. Generally speaking, the material hardens and becomes brittle owing to this relaxation (Hutchinson, 1973). For the mechanism behind the secondary relaxation, Jones (1985) proposed a theory of structural change caused by a flip rotation of the phenyl ring in the main molecular chain for a bisphenol A - PC. Ree and Eyring (1955)

formulated a relationship between the stress and strain rate for a polymer, using a hyperbolic sine function and proposed to represent the total stress as the sum of the stress in each relaxation process. By adding the effect of temperature on yield stress to this theory, Bauwens (1972) explained changes in the yield stress and loss tangent within the range of temperature and strain rate at which secondary relaxation occurs. Mulliken and Boyce (2006) formulated a three-dimensional constitutive model for secondary relaxation by embedding the previously proposed model, which can express the strain softening behavior of polymers, into the five-elements parallel model, and then tried to explain the nonlinear relationship between the yield stress and strain rate of PC obtained in experiments. However, the formulation of the plastic shear strain rate was used in different forms of the high-precision formulation by Argon (1973), and it can be said that such a theoretical basis is poor.

In this study, a bulk specimen made of two types of commercial epoxy resin structural adhesives is manufactured after solidification. Using this specimen, a compressive test using an INSTRON-type material testing machine and a split Hopkinson pressure bar method (Kolsky, 1949; Nemat-Nasser et al., 1991; Yokoyama and Shimizu, 1998; Sato and Ikegami, 1999, 2001; Nakai and Yokoyama, 2008) is carried out to investigate the stress - strain curve in a wide range of strain rate. After that, the nonlinear relationship between the yield stress and strain rate is shown. Since it is assumed that the yield stress at a high strain rate is dominated by secondary relaxation and the mechanism of this secondary relaxation is the presence of rotational degrees of freedom, on the basis of Jones' explanation (Jones, 1985), the plastic shear strain rate for the secondary relaxation is formulated on the basis of an expansion of Argon's formalism (Argon, 1973) using an idea presented by Li and Gilman (1970). In addition, total shear stress is expressed using the parallel two-elements model, as was done by Ree and Eyring (1955), with the proposed model and using the generalized model of Argon's formula (Argon, 1973; Boyce et al., 1988).

Taking into account that the amorphous glassy polymer after solidification of the adhesive, a rate form of the three-dimensional constitutive equation is formulated on the basis of a four-elements model including an elastic series element. First, the plastic deformation rate tensor for each relaxation process is formulated by using the effective stress, which represents the difference between total stress, back stress and the stress at each relaxation process, and the formulated plastic shear strain rate. The back stress, which represents the resistance against the orientation of the

molecular chain network, can be calculated using a previously proposed model (Haward and Thackray, 1968; Boyce et al., 1988; Arruda and Boyce, 1991; Tomita, 2000). Under the assumption that the plastic deformation rate tensors in individual relaxation processes are the same, a nonlinear simultaneous equation for the stress tensor in each relaxation process can be obtained. When a generalized Hooke's law is included, the rate form of a three-dimensional constitutive equation can be derived. The proposed constitutive equation is implemented into the commercial finite element code ABAQUS / Explicit and then a finite element simulation is performed. Finally, the validity of the formulated model is shown by comparison with the experimental result.

## **2. EXPERIMENTAL PROCEDURES**

### **2.1 Preparation of Specimen**

The structural adhesives used in this study are an epoxy resin thermosetting adhesive (Scotch-Weld 1838 by 3M, hereafter abbreviated to SW1838) and a CTBN-modified epoxy resin adhesive (DP-460 by 3M). Here, CTBN stands for carboxyl-terminated butadiene-acrylonitrile rubber, and the ductile phase is formed by a microscopic phase separation of CTBN incorporated into the epoxy structural adhesive during solidification to provide toughness and ductility. Actually, this adhesive is superior in ductility and toughness compared with SW1838 from the catalog. The appropriate weights of base and accelerator resins are mixed and injected into a clear syringe (PSY - 10E manufactured by Musashi Engineering, Inc.). After a defoaming procedure of the syringe filled of adhesive using the defoaming machine (THINKY Corporation, AR-100), the syringe is placed into a vacuum desiccator and cured at room temperature for 24 hs. The specimen is machined into a solid cylinder 14 mm in diameter and 7 mm in thickness from the cured syringe. In addition, a postcuring procedure in an electric furnace at 338 K for 2 hs in the case of SW1838 and 322 K for 3 hs in the case of DP - 460 is applied and then both edges of the specimen are polished with abrasive paper with a grit number of 2000#.

To verify the amorphous state of a specimen obtained as described above, a differential scanning calorimeter (DSC-220C manufactured by SEIKO Instruments Inc.) is used for thermal analysis of the adhesive. Figure 1 represents the relationships between the heat flow and temperature of (a) SW1838 and (b) DP - 460 obtained by DSC

analysis. The different lines correspond to the number of trials. As shown in this figure, it can be seen that the negative peaks are at about 345 K for both adhesives and the reproducibility with respect to the peaks is good. Since the glass transition temperatures of SW1838 and DP-460 are 328 and 333 K from the catalog, it can be confirmed that this DSC analysis is valid. As the result, the specimens are in the amorphous glassy state below this temperature with the negative peak of heat flow. At a lower temperature from the peak, sudden decreases in heat flow near 280 K for SW1838 and 260 K for DP-460 appear. This phenomenon is related to a secondary relaxation known as  $\beta$ -relaxation. Again, the prepared specimen, which will be used in the experiment at room temperature, is in the glassy state and undergoes secondary relaxation.

## 2.2 Quasi-static and Impact Compressive Experiments

The quasi-static to dynamic compressive tests in the strain rate range from  $10^{-4}$  to  $1 \text{ s}^{-1}$  are carried out using an INSTRON-type material testing machine (Autograph AG-1 250kN manufactured by Shimadzu Corporation) at room temperature. To avoid a beer-barreled deformation due to the effect of friction between a surface of the die and the two ends of the specimen, commercial graphite grease is applied to the surface.

Impact tests in the strain rate range from  $10^2$  to  $10^3 \text{ s}^{-1}$  are carried out using a split Hopkinson pressure bar apparatus at room temperature. Figure 2 shows a schematic illustration of the split Hopkinson pressure bar apparatus used here. In consideration of a lower mechanical impedance of the specimen, extra super duralumin A7075-T6511 (JIS) is chosen as the material for the striker, and input and output stress bars. Four semiconductor strain gauges (Kyowa Electric instruments Co., Ltd., KSP-2-120-E4) are glued at the middle position on the input and output rods in order to eliminate flexural strain. The specimen for the impact compressive test is placed between input and output bars through graphite grease and commercial molybdenum disulfide to avoid beer-barreled deformation. The striker is launched using compressed air and hits the left side of input bar. The specimen undergoes an impact compressive load indirectly by the incident strain wave  $\varepsilon_i(t)$ . The generated incident wave propagates from left to right in the input bar, some of the incident wave is reflected  $\varepsilon_r(t)$  at the interface between the specimen and the input bar, and the rest of the wave is transmitted  $\varepsilon_t(t)$  to the output bar. On the basis of the theory of elastic wave

propagation in one dimension, assuming dynamic stress equilibrium in the specimen, nominal stress  $\sigma_n(t)$  and nominal strain  $\varepsilon_n(t)$  of the specimen can be calculated by using a time series of the recorded strain signals, as in the

$$\sigma_n(t) = \frac{AE}{2a} \{\varepsilon_i(t) + \varepsilon_r(t) + \varepsilon_t(t)\}, \quad \dot{\varepsilon}_n(t) = \frac{c_0}{\ell} \{\varepsilon_i(t) - \varepsilon_r(t) - \varepsilon_t(t)\}, \quad \varepsilon_n(t) = \int_0^t \dot{\varepsilon}_n(t') dt', \quad (1)$$

where  $E$ ,  $c_0$  and  $A$  are the Young's modulus, the wave velocity and the cross-sectional area of the stress bars, respectively.  $a$  and  $\ell$  are the cross-sectional area and the length of the specimen. True stress  $\sigma(t)$  can be calculated from  $\sigma_n(t)$  and  $\varepsilon_n(t)$  by the conventional way under an assumption of a constant volume during deformation. Of course, the increase of cross section in the specimen cannot be measured during the impact deformation. The polymeric materials might introduce the volume change during deformation. From this point of view, it is noted that true stress calculated such a way is not correct. Generally speaking, the duration of the transmitted and reflected strain waves becomes longer than that of the incident wave as the result of a long relaxation time for the polymeric material. In the impact testing of polymeric materials, it is well known that the time taken to reach dynamic stress equilibrium at the ends of the specimen also becomes longer than the time required for metallic materials, because of the inclusion of relaxation time. In this study, the incident wave is controlled by attaching a thin disk (5 mm in diameter and 0.5 mm in thickness) made of pure copper C1100 (JIS) as a buffer to the left side of the input bar; i.e. this is the pulse shaping technique (Nemat-Nasser et al., 1991; Nakai and Yokoyama, 2008), and is necessary to lengthen the rise time of the incident wave.

### 3. EXPERIMENTAL RESULTS

To confirm the effectiveness of the pulse shaping technique, Figure 3 shows the output signal from the strain gauges glued on to the input and output stress bars (a) without a pulse shaper and (b) with a pulse shaper. In this figure, the rise time of the incident wave becomes longer, and extra oscillation can be removed by introducing the pulse shaper. The reflected wave can be smoothed and the initial peak of the reflected wave can be reduced. As a result, the wave becomes almost constant. This means that a constant nominal strain rate can be realized during the impact compression test. The transmitted wave remains almost the same after introducing the pulse shaper. Figure 4 shows a

comparison of the time series of the loads acting on the two sides of the specimen during impact compression test (a) with the pulse shaper and (b) without the pulse shaper. According to the propagation theory of the one-dimensional elastic wave, the loads can be calculated using the following equation with the measured strain waves.

$$P_1(t) = AE\{\varepsilon_i(t) + \varepsilon_r(t)\}, \quad P_2(t) = AE\varepsilon_r(t) \quad (2)$$

As shown in Fig. 4(a), the difference between the loads at the two ends of the specimen can be observed, and the equilibrium state cannot be reached if there is no pulse shaper. However, once the pulse shaper is introduced, the equilibrium state is maintained during the deformation because the loads are similar, as shown in Fig. 4 (b). As a result, the validity and necessity of the pulse shaping technique can be confirmed.

Figure 5 shows true stress - true strain curve obtained from the quasi-static impact and compression tests for (a) SW1838 and (b) DP-460. The two kinds of epoxy structural adhesives used in this study show a linear elastic region at first, then a maximum stress similar to the yield point, and finally a strain softening behavior. Ultimately, the strain hardening behavior can be observed. When the maximum stress (hereafter called the yield stress) is focused on, the increase in it is constant with increasing strain rate in the region from quasi-static to dynamic deformation. However, the yield stress increases rapidly against the increase of the strain rate under impact deformation. In our experiment for quasi-static case, no clear instability like neck propagation in tension can be observed from the surface of specimen. However, the instability might be occurred because the strain-softening region was captured in the stress-strain curve.

To visualize the above-described characteristics clearly, Fig. 6 shows the semi-logarithmic relationship between the yield stress and strain rate obtained from the experiments and analysis described later. In the figure, open circles represent the experimental results. In the experimental results, yield stress increases linearly with increasing strain rate from the quasi-static to dynamic range, as described above. However, the slope of the linear region at a low strain rate is not inherited at a high strain rate; the curve is expressed by different relatively steep lines. Overall, nonlinearity of the yield stress - strain rate curve can be observed. As a result, stress - strain relationship shown in Fig. 5 and the yield stress - strain rate relationship shown in Fig. 6 can be also seen in other amorphous glassy polymers such as the PC and PMMA. The results suggest that the constitutive model of other glassy polymers can be applied to

describe the deformation behavior of the bulk epoxy adhesive material after solidification.

Meanwhile, Argon (1973) formulated the activated free energy of the intermolecular resistance caused by a rotation in segments of the molecular chain, using the analytical results obtained by Li and Gilman (1970), when a shear stress  $\tau^*$  was applied to a molecular chain with a double kink, as shown in Fig. 7. As a result, the relationship between the plastic shear strain rate  $\dot{\gamma}^p$  and  $\tau^*$  was determined from the change in the activated free energy considering the effect of pressure, using the following equation,

$$\dot{\gamma}^p = \dot{\gamma}_0 \exp \left[ -\frac{3\pi G \omega^2 a^3}{16(1-\nu)k_B T} \left\{ 1 - 8.5(1-\nu)^{\frac{5}{6}} \left( \frac{\tau^*}{G} \right)^{\frac{5}{6}} \right\} - \frac{0.15Ga^3(\omega - \omega_c)^2}{k_B T} \left( \frac{p}{G} \right) \right]. \quad (3)$$

Here,  $G(T)$  and  $\nu(T)$  are the shear modulus and Poisson's ratio as a function of the absolute temperature  $T$ ,  $\omega$  is the rotational angle in the activated configurations from the initial state,  $a$  is the mean radius of the molecular chain,  $p$  is the hydrostatic pressure,  $k_B$  is the Boltzmann constant, and  $\dot{\gamma}_0$  and  $\omega_c$  are constants. Boyce et al. (1988) expanded the above formula by arranging these parameters and vanishing the term containing  $p$ , as in the following equation,

$$\dot{\gamma}^p = \dot{\gamma}_0 \exp \left[ -\frac{As_0}{T} \left\{ 1 - \left( \frac{\tau^*}{s_0} \right)^{\frac{5}{6}} \right\} \right], \quad s_0 \equiv \frac{0.077G}{(1-\nu)} \quad \text{and} \quad A \equiv \frac{39\pi\omega^3 a^3}{16k_B}. \quad (4)$$

The analytical results obtained for SW1838 and DP-460 using Eq. (4) are shown as solid and dashed lines on Fig. 6. In this figure, experimental and analytical results show good correspondence at low strain rates. However, it is extremely difficult to represent this phenomenon by using Eq. (4) since Eq. (4) does not fit at all the results at high strain rate.

## 4. CONSTITUTIVE FORMULATION

### 4.1 Plastic Shear Strain Rate for Secondary Relaxation

Here, the plastic shear strain rate is formulated by considering that the deformation of the polymeric material at a high strain rate will be dominated by a secondary relaxation called the  $\beta$ -relaxation (Hutchinson, 1973) and the adhesives used in this research work show the  $\beta$ -relaxation as mentioned above. First, the mechanism for secondary relaxation proposed by Jones (1985), i.e., the relaxation caused by the existence of rotational

degrees of freedom in the main molecular chain, is supported and the formulation of the plastic shear strain rate in the case of only secondary relaxation is given. Now, let us consider that a molecular chain with average molecular radius  $a$ , constant rotation angle  $\omega$  and chain length  $z$  of a segment in the equilibrium configuration, as shown on Fig. 7, undergoes the torsional degrees of freedom  $\theta$ , as shown in Fig. 8, as in Argon's interpretation (Argon, 1973). Of course, Argon (1973) represents the rotation of the main molecular chain by  $\omega$ . However, it can be expressed by  $\theta$  since structural changes during the  $\beta$ -relaxation due to a flip motion of a phenyl ring shown by Jones (1985) is likely to be caused by twisting, not the bending degree of freedom  $\omega$ .

Li and Gilman (1970) derived the following free energy of the molecular chain, which undergoes torsion, including the interaction between the chains

$$\Delta F = \Delta F(\theta) = \frac{3\pi a^3 G \theta^2}{16} - \frac{3\pi a^3 G \theta^2}{8} \left(\frac{a}{z}\right)^5. \quad (5)$$

A shear stress  $\tau_\beta$  is applied to a rectangular region of an aggregate of chains, similar to Argon (1973), as shown in Fig. 8. In this case, normal strain  $\varepsilon_{22}$  in the vertical direction (direction 2 in the figure) can be expressed as

$$\varepsilon_{22} = -\frac{2a\ell}{LA} z \sin \omega (1 - \cos \theta), \quad (6)$$

where  $L$  and  $A$  are the length and the cross-sectional area of the region, respectively, and  $\ell$  is the average length of the chain along direction 1 in the figure. Assuming plane strain, normal strain in the horizontal direction (direction 3 in Fig. 8)  $\varepsilon_{33}$  for a constant volume during plastic deformation can be expressed as

$$\varepsilon_{33} = -\varepsilon_{22} = \frac{2a\ell}{LA} z \sin \omega (1 - \cos \theta). \quad (7)$$

The work  $\Delta W$  by applied shear stress  $\tau_\beta$  can be written as

$$\Delta W = [4a\ell z \sin \omega (1 - \cos \theta)] \tau_\beta. \quad (8)$$

From Eqs. (1) and (8), free energy  $\Delta G$  can be expressed as

$$\Delta G = \Delta F - \Delta W = \frac{3\pi a^3 G \theta^2}{16} - \frac{3\pi a^3 G \theta^2}{8} \left(\frac{a}{z}\right)^5 - 4a^2 \ell \left(\frac{z}{a}\right) \sin \omega \tau_\beta (1 - \cos \theta). \quad (9)$$

In addition, since a change in  $\theta$  from  $-\pi/2$  to  $\pi/2$  should be considered,  $\cos\theta$  in the above equation can be expressed approximately as

$$1 - \cos\theta \cong \frac{1}{2}\theta^2 - \frac{1}{24}\theta^4. \quad (10)$$

Thus,  $\Delta G$  can be rewritten under the above approximation as

$$\Delta G = \left[ \frac{3\pi a^3 G}{16} - \frac{3\pi a^3 G}{8} \left(\frac{a}{z}\right)^5 - 2a^2 \ell \left(\frac{z}{a}\right) \sin \omega \tau_\beta \right] \theta^2 + \frac{a^2 \ell \sin \omega}{6} \left(\frac{a}{z}\right) \tau_\beta \theta^4. \quad (11)$$

Now, the degree of freedom to be considered here is only  $\theta$ , and hence the extremal problem of  $\Delta G$  on  $\theta$  is considered. Therefore,  $\theta_{eq}$  in the activated configuration is obtained as

$$\theta_{eq} = 0, \pm \sqrt{6 - \frac{9\pi a G}{8(z/a)\tau_\beta \ell \sin \omega} \left[ 1 + \frac{2}{(z/a)^5} \right]}. \quad (12)$$

Since  $\theta_{eq} = 0$  will be a saddle point, free energy at the stable configuration  $\Delta G_\beta^*$  can be formulated as

$$\Delta G_\beta^* = \frac{3a^2}{128\ell(z/a)^{11}} \left\{ 48\pi a G \ell \left[ \left(\frac{z}{a}\right)^5 - 2 \right] \left(\frac{z}{a}\right)^6 - \frac{9\pi^2 a^2 G^2 \left[ (z/a)^5 - 2 \right]^2}{\tau_\beta \sin \omega} - 256\ell^2 \left(\frac{z}{a}\right)^6 \sin \omega \tau_\beta \right\}. \quad (13)$$

The plastic shear strain rate in the secondary relaxation process can be derived from the same procedure as used by Argon (1973) and Boyce et al. (1988) as

$$\dot{\gamma}_\beta^p = \dot{\gamma}_{0\beta}^p \exp \left\{ - \frac{9\pi a^3 G \left[ (z/a)^5 - 2 \right] \left(\frac{a}{z}\right)^5}{8k_B T} \left[ 1 - \frac{3\pi a \left\{ (z/a)^5 - 2 \right\} \left(\frac{a}{z}\right)^6 \left(\frac{G}{\tau_\beta}\right) - \frac{16\ell \sin \omega}{3\pi a \left\{ (z/a)^5 - 2 \right\} \left(\frac{\tau_\beta}{G}\right)} \right] \right\}. \quad (14)$$

By an arrangement of parameters in the above equation similar to that adopted by Boyce et al. (1988), the following simplified equation can be obtained:

$$\dot{\gamma}_\beta^p = \dot{\gamma}_{\beta 0}^p \exp \left\{ - \frac{A_\beta s_{\beta 0}}{T} \left( 1 - \frac{\tau_\beta}{s_{\beta 0}} - \frac{s_{\beta 1}}{\tau_\beta} \right) \right\}, \quad (15)$$

$$s_{\beta 0} \equiv \frac{3\pi a G \left\{ (z/a)^5 - 2 \right\}}{16\ell \sin \omega}, \quad s_{\beta 1} \equiv s_{\beta 0} \left(\frac{a}{z}\right)^6 \quad \text{and} \quad A_\beta \equiv \frac{6\pi a^2 \ell \sin \omega}{k_B} \left(\frac{a}{z}\right)^5.$$

It is noted that the expressions given by Mulliken and Boyce (2006) are different from Eqs. (4) and (15) if they are

employed to express the primary and the secondary relaxation process, respectively. In addition, if  $\tau_\alpha$  is assumed to be the shear stress driving the plastic shear strain rate  $\dot{\gamma}_\alpha^p$  during the primary relaxation, total shear stress  $\tau$  can be expressed, following Ree and Eyring (1955), as

$$\tau = \tau_\alpha + \tau_\beta. \quad (16)$$

In this case,  $\dot{\gamma}_\alpha^p = \dot{\gamma}_\beta^p = \dot{\gamma}^p$  is assumed because the above equation is based on a parallel two-elements model. Equations (4) and (15) are solved for  $\tau_\alpha$  and  $\tau_\beta$ , and then  $\tau$  can be calculated as the sum of the shear stresses, as described by Eq. (16), as

$$\tau = s_{\alpha 0} \left\{ 1 - \frac{T}{A_\alpha s_{\alpha 0}} \ln \left( \frac{\dot{\gamma}^p}{\dot{\gamma}_{\alpha 0}^p} \right) \right\}^{6/5} + \frac{1}{2} \left\{ s_{\beta 0} + \frac{T}{A_\beta s_{\beta 0}} \ln \left( \frac{\dot{\gamma}^p}{\dot{\gamma}_{\beta 0}^p} \right) + \sqrt{\left[ s_{\beta 0} + \frac{T}{A_\beta s_{\beta 0}} \ln \left( \frac{\dot{\gamma}^p}{\dot{\gamma}_{\beta 0}^p} \right) \right]^2 - 4s_{\beta 0}s_{\beta 1}} \right\}. \quad (17)$$

In this case, seven parameters,  $s_{\alpha 0}$ ,  $s_{\beta 0}$ ,  $s_{\beta 1}$ ,  $A_\alpha$ ,  $A_\beta$ ,  $\dot{\gamma}_{\alpha 0}^p$  and  $\dot{\gamma}_{\beta 0}^p$ , must be identified from the experimental results. However, the total number of parameters is reduced to six since  $s_{\alpha 0}$  can be expressed by Eq. (4).

In order to check the validity of Eq. (17), Figure 9 shows the semi-logarithmic relationship between the yield stress and strain rate obtained experimentally and using Eq. (17). In the figure, the open circles and triangles indicate experimental results. A trial and error procedure is required to fit the experimental data by operating six parameters as mentioned above. The solid and dashed lines indicate the analytical results obtained using Eq. (17). For the calculation of the analytical result using Eq. (17), the elastic shear strain is assumed to be negligibly small. The shear stress and shear strain rate are converted to normal stress and normal strain rate using the relationships  $\sigma = \sqrt{3}\tau$  and  $\dot{\epsilon} = \dot{\gamma} / \sqrt{3}$ , respectively. In this figure, a fairly good agreement can be observed for the two adhesives.

#### 4.2 Kinetics of Polymeric Materials Given by Boyce et al. (1998)

This section describes the kinetics of polymeric materials obeying the description by Boyce et al. (1998). Let us consider that the initial isotropic glassy polymers are deformed following the deformation gradient  $F_{ij}$  at a time defined by

$$F_{ij} = \frac{\partial x_i}{\partial X_j}, \quad (18)$$

where  $X_i$  is the reference configuration, and  $x_i$  represents the current configuration. At the reference configuration, the glassy polymeric material is in an isotropic state in which molecular chains are randomly oriented.  $F_{ij}$  can be multiplicatively decomposed into the elastic component  $F_{ij}^e$  and plastic component  $F_{ij}^p$ , as shown by the equation below:

$$F_{ij} = F_{ik}^e F_{kj}^p. \quad (19)$$

$F_{ij}^p$  represents the stress-free configuration under the complete unloading condition and a permanent degree of molecular orientation in the material is indicated physically.  $F_{ij}$  is expressed in the form of the following equation using elastic stretch  $V_{ij}^e$ , rotation  $R_{ij}$  and plastic stretch  $U_{ij}^p$ :

$$F_{ij} = V_{ik}^e R_{kl} U_{lj}^p. \quad (20)$$

$R_{ij}$  is assumed to be divided into an elastic part and a plastic part, similarly to  $F_{ij}$ , as

$$R_{ij} = R_{ik}^e R_{kj}^p. \quad (21)$$

The following equation can be obtained by polar decomposition and using Eq. (21).

$$F_{ij}^e = V_{ik}^e R_{kj}^e = R_{ik}^e U_{kj}^e \quad \text{and} \quad F_{ij}^p = V_{ik}^p R_{kj}^p = R_{ik}^p U_{kj}^p. \quad (22)$$

In reality, we cannot specify whether rotation is elastic or plastic. However, the next equations are assumed here.

$$R_{ij}^e = \delta_{ij} \quad \text{and} \quad R_{ij} = R_{ij}^p. \quad (23)$$

As a result, we can derive

$$F_{ij}^p = V_{ik}^p R_{kj} = R_{ik} U_{kj}^p. \quad (24)$$

The above equation expresses the stress-free configuration obtained after unloading without rotation, and  $F_{ij}^e = F_{ji}^e$  can be satisfied. Next, the velocity gradient  $L_{ij}$  can be obtained as

$$L_{ij} = \frac{\partial v_i}{\partial x_j} = d_{ij} + \omega_{ij} = \dot{F}_{ik} F_{kj}^{-1} = \dot{F}_{ik}^e F_{kj}^{e-1} + F_{ik}^e \dot{F}_{kl}^p F_{lm}^{p-1} F_{mj}^{e-1}, \quad (25)$$

where  $v_i$  is the velocity,  $d_{ij}$  is the deformation rate tensor which is a symmetric part of  $L_{ij}$  and  $\omega_{ij}$  is the spin tensor which is an antisymmetric part of  $L_{ij}$ . In addition, the following equations are obtained by assuming that  $d_{ij}$  and  $\omega_{ij}$  are the sum of the elastic and plastic components.

$$d_{ij} = d_{ij}^e + d_{ij}^p, \quad \omega_{ij} = \omega_{ij}^e + \omega_{ij}^p, \quad (26)$$

$$d_{ij}^e + \omega_{ij}^e = \dot{F}_{ik}^e F_{kj}^{e-1} \quad \text{and} \quad d_{ij}^p + \omega_{ij}^p = F_{ik}^e \dot{F}_{kl}^p F_{lm}^{p-1} F_{mj}^{e-1}. \quad (27)$$

The velocity gradient in the stress-free configuration  $L_{ij}^p$  is given by

$$L_{ij}^p = \dot{F}_{ik}^p F_{kj}^{p-1} = \tilde{d}_{ij}^p + \tilde{\omega}_{ij}^p. \quad (28)$$

Strictly speaking, the plastic deformation rate tensors in the loading and unloading configurations can be expressed as

$$d_{ij}^p = \frac{1}{2} (F_{ik}^e L_{kl}^p F_{ij}^{e-1} + F_{jk}^e L_{kl}^p F_{li}^{e-1}) \quad \text{and} \quad \tilde{d}_{ij}^p = \frac{1}{2} (L_{ij}^p + L_{ji}^p). \quad (29)$$

They are different only in  $F_{ij}^e$ ; however, the magnitude of each component in  $F_{ij}^e$  is equivalent to the elastic strain, and here, the following equation can be satisfied since  $F_{ij}^e$  is negligibly small

$$\tilde{d}_{ij}^p \equiv d_{ij}^p \equiv \hat{d}_{ij}^p. \quad (30)$$

Also, by ignoring the elastic deformation gradient, we can approximate  $F_{ij}^p$  and  $\omega_{ij}^p$  as

$$\omega_{ij}^p = \omega_{ij} \quad \text{and} \quad F_{ij}^p = F_{ij}. \quad (31)$$

Plastic deformation rate tensor  $\hat{d}_{ij}^p$  can be expressed generally in each case of a loading or unloading configuration as

$$\hat{d}_{ij}^p = \dot{\gamma}^p N_{ij}, \quad (32)$$

where  $\dot{\gamma}^p$  is the equivalent plastic shear strain rate and  $N_{ij}$  is the tensor indicating the direction. Generally speaking, since there are an associative and a non-associative cases for  $N_{ij}$ . Our choice is described later.

## 4.2 Rate Form of Three-dimensional Constitutive Equation

The resistance to a plastic flow of glassy polymeric materials is assumed to be divided into two different physical resistances, the intermolecular resistance related to the rotation of the chain segments and the resistance of the molecular orientation (Boyce et al, 1988; Tomita, 2000). Figure 10 shows the four-elements model with three parallel elements and one elastic series element used in this study. Here, the intermolecular resistance at each relaxation process represented using the subscript  $\alpha$  or  $\beta$  is expressed by a nonlinear dashpot. The eight-chain model proposed by Arruda and Boyce (1991) is used for the resistance of the molecular orientation. In the previous section, the intermolecular resistance in the primary and secondary relaxations, as shown in Figure 8, can be considered to be caused by the rotational deformation of the double-kinked molecular chain, including bending and twisting. Then,

the relationship between the shear stress and the plastic shear strain rate is formulated. To describe the two effects of strain softening and pressure in the model proposed in the previous section, the parameters  $s_{\alpha 0}$  and  $s_{\beta 0}$  in Eqs. (4) and (15) are replaced, as was done by Boyce et al. (1988), as

$$\dot{\gamma}_{\alpha}^p = \dot{\gamma}_{\alpha 0} \exp \left[ -\frac{\Delta G_{\alpha 0}^*}{T} \left\{ 1 - \left( \frac{\tau_{\alpha}}{s_{\alpha} + \alpha_{\alpha} P} \right)^{\frac{5}{6}} \right\} \right], \quad \dot{\gamma}_{\beta}^p = \dot{\gamma}_{\beta 0} \exp \left\{ -\frac{\Delta G_{\beta 0}^*}{T} \left( 1 - \frac{\tau_{\beta}}{s_{\beta} + \alpha_{\beta 0} P} - \frac{\hat{s}_{\beta} + \alpha_{\beta 1} P}{\tau_{\beta}} \right) \right\}, \quad (33)$$

where  $\alpha_{\alpha}$  and  $\alpha_{\beta}$  are the pressure coefficients in each relaxation process, and  $\Delta G_{\alpha 0}^* = s_{\alpha 0} A_{\alpha}$  and  $\Delta G_{\beta 0}^* = s_{\beta 0} A_{\beta}$  are the constants resulting from the rearrangement of the parameters.  $s_{\alpha}$ ,  $s_{\beta}$  and  $\hat{s}_{\beta}$  are new state variables that represent the current structure with their initial values being  $s_{\alpha 0}$ ,  $s_{\beta 0}$  and  $s_{\beta 1}$ . Similar to the work of Boyce et al. (1988), their evolution equations are assumed to be written as

$$\dot{s}_{\alpha} = h_{\alpha} \left\{ 1 - \frac{s_{\alpha}}{s_{ss,\alpha}(T, \dot{\gamma}_{\alpha}^p)} \right\} \dot{\gamma}_{\alpha}^p, \quad \dot{s}_{\beta} = h_{\beta} \left\{ 1 - \frac{s_{\beta}}{s_{ss,\beta}(T, \dot{\gamma}_{\beta}^p)} \right\} \dot{\gamma}_{\beta}^p \quad \text{and} \quad \dot{\hat{s}}_{\beta} = \hat{h}_{\beta} \left\{ 1 - \frac{\hat{s}_{\beta}}{\hat{s}_{ss,\beta}(T, \dot{\gamma}_{\beta}^p)} \right\} \dot{\gamma}_{\beta}^p. \quad (34)$$

$h_{\alpha}$ ,  $h_{\beta}$  and  $\hat{h}_{\beta}$  are the positive constants.  $s_{ss,\alpha}$ ,  $s_{ss,\beta}$  and  $\hat{s}_{ss,\beta}$  are the values of  $s_{\alpha}$ ,  $s_{\beta}$  and  $\hat{s}_{\beta}$  in the equilibrium state and have values less than  $s_{\alpha 0}$ ,  $s_{\beta 0}$  and  $s_{\beta 1}$ , respectively. Since it is sufficient that the strain softening behavior and pressure effect in the secondary relaxation can be expressed using only  $s_{\beta}$ ,  $\hat{s}_{\beta}$  is dealt with as a constant here.

With continuing plastic deformation, the molecular chain becomes oriented in the direction of plastic stretch and a back stress is generated in the network structure, which consists of molecular chains (Haward and Thackray, 1968). This back stress becomes a kind of resistance to further plastic deformation. Using the eight-springs molecular chain model (Arruda and Boyce, 1991), in which molecular chains are fixed to each other at both ends, the principal component of back stress (Boyce et al., 1988; Arruda and Boyce, 1991; Tomita, 2000) is expressed as

$$b_i = \frac{1}{3} C^R \sqrt{N} \frac{V_i^{p^2} - \lambda_c^2}{\lambda_c} L^{-1} \left( \frac{\lambda_c}{\sqrt{N}} \right). \quad (35)$$

Here,  $C^R = nk_B T$ ,  $n$  is the number of chains per unit volume,  $N$  is a number of rigid chain links between entanglements and its root is a limit stretch of the chain, and  $\lambda_c$  is the principal plastic stretch that can be expressed by

$$\lambda_c^2 = \frac{1}{3}(V_1^{p^2} + V_2^{p^2} + V_3^{p^2}). \quad (36)$$

$L^{-1}(\lambda_c / \sqrt{N}) = \beta_c$  is the inverse of the Langevin function defined as

$$L(\beta_c) = \coth \beta_c - \frac{1}{\beta_c} = \frac{\lambda_c}{\sqrt{N}}. \quad (37)$$

Since back stress  $b_{ij}$  is defined in the unloading configuration and develops with plastic stretch, it can be calculated as being coaxial with plastic left stretch  $V_{ij}^p$  obtained by polar decomposition of the plastic deformation gradient:

$$b_{ij} = \frac{1}{3} C^R \frac{\sqrt{N}}{\lambda_c} L^{-1}\left(\frac{\lambda_c}{\sqrt{N}}\right) (B_{ij} - \lambda_c^2 \delta_{ij}), \quad (38)$$

where  $B_{ij} = F_{ik} F_{jk}$  and  $\lambda_c^2 = \frac{1}{3} B_{ii}$ . In the above equation, the following is used under an assumption that the elastic

deformation is negligibly small.

$$V_{ij}^p \approx B_{ij}^{1/2} \quad (39)$$

The back stress tensor at the current configuration  $\sigma_{ij}^B$  can be written as

$$\sigma_{ij}^B = \frac{1}{\det F_{ij}^e} F_{ik}^e b_{kl} F_{lj}^e. \quad (40)$$

Following the work of Boyce et al. (1988), the plastic deformation rate tensor at each relaxation process can be expressed from Eq. (32) with the associated flow rule, by using the back stress tensor and the plastic shear strain rate, as

$$d_{ij}^{p\alpha} = \dot{\gamma}_\alpha^p \frac{\sigma_{ij}^{\alpha'}}{\sqrt{2}\tau_\alpha}, \quad d_{ij}^{p\beta} = \dot{\gamma}_\beta^p \frac{\sigma_{ij}^{\beta'}}{\sqrt{2}\tau_\beta}, \quad (41)$$

where  $(\cdot)'$  means the deviatoric tensor, and  $\sigma_{ij}^\alpha$  and  $\sigma_{ij}^\beta$  are the driving stress for each relaxation process, which can be calculated as

$$\sigma_{ij} = \sigma_{ij}^\alpha + \sigma_{ij}^\beta + \sigma_{ij}^B, \quad (42)$$

where  $\sigma_{ij}$  is the total Cauchy stress.  $\tau_\alpha$  and  $\tau_\beta$  can be calculated using  $\sigma_{ij}^{\alpha'}$  and  $\sigma_{ij}^{\beta'}$  as

$$\tau_\alpha = \sqrt{\frac{1}{2} \sigma_{ij}^{\alpha'} \sigma_{ij}^{\alpha'}}, \quad \tau_\beta = \sqrt{\frac{1}{2} \sigma_{ij}^{\beta'} \sigma_{ij}^{\beta'}}. \quad (43)$$

On the basis of Fig. 10, the total deformation rate tensor can be decomposed into three parts:

$$d_{ij} = d_{ij}^e + d_{ij}^p + d_{ij}^h, \quad (44)$$

where  $d_{ij}^h$  is the thermal part of the deformation rate tensor defined as

$$d_{ij}^h = A_{ij} \dot{T}, \quad A_{ij} = \Delta v_h \delta_{ij}, \quad (45)$$

where  $\Delta v_h$  is the thermal expansion coefficient. From Hooke's law, the following constitutive equation for elastic deformation can be satisfied.

$$\overset{\circ}{S}_{ij} = C_{ijkl}^e d_{kl}^e, \quad C_{ijkl}^e = 2G \left\{ \frac{1}{2} (\delta_{ik} \delta_{jl} + \delta_{il} \delta_{jk}) + \frac{\nu}{(1-2\nu)} \delta_{ij} \delta_{kl} \right\}. \quad (46)$$

Here,  $\overset{\circ}{S}_{ij}$  is an objective rate of the Kirchhoff stress tensor. In this study, the Green-Nagdhi rate defined as follows is chosen.

$$\overset{\circ}{S}_{ij} \equiv \dot{S}_{ij} - \Omega_{ik} S_{kj} + S_{ik} \Omega_{kj} \quad (47)$$

Here,  $\Omega_{ij} = \dot{R}_{ik} R_{jk}$ . Assuming  $d_{ij}^{p\alpha} = d_{ij}^{p\beta} = d_{ij}^p$ , the following rate form of the constitutive equation can be obtained:

$$\overset{\circ}{S}_{ij} = D_{ijkl}^e d_{kl}^e - \dot{\gamma}_\alpha^p P_{ij}^\alpha - B_{ij}^e \dot{T}, \quad (48)$$

where  $P_{ij}^\alpha$  can be calculated as

$$P_{ij}^\alpha = \frac{1}{\sqrt{2} \tau_\alpha} C_{ijkl}^e \sigma_{kl}^{\alpha'} = \frac{\sqrt{2} G}{\tau_\alpha} \sigma_{kl}^{\alpha'}. \quad (49)$$

In the constitutive equation,  $\sigma_{ij}^{\alpha'}$  and  $\sigma_{ij}^{\beta'}$  become undetermined variables; however, the unknown variables can be calculated by the solution of the following equation derived from Eqs. (41) and (42), and  $d_{ij}^{p\alpha} = d_{ij}^{p\beta} = d_{ij}^p$ .

$$\left( 1 + \frac{\dot{\gamma}_\alpha^p \tau_\beta}{\dot{\gamma}_\beta^p \tau_\alpha} \right) \sigma_{ij}^{\alpha'} = \sigma_{ij}^{\beta'} - \sigma_{ij}^{B'}. \quad (50)$$

Actually, Eq. (50) is not a single equation and contains six equations by considering symmetry of the deviatoric stress tensor. Additionally, Eq. (50) with Eqs. (33) and (43) becomes a nonlinear simultaneous equation of  $\sigma_{ij}^{\alpha'}$ .  $\sigma_{ij}^{\beta'}$  can

be calculated from Eq. (42). This nonlinear equation can be solved numerically by the Newton-Raphson method.

## 5. COMPUTATIONAL CONDITION, RESULTS AND DISCUSSION

The commercial finite element code ABAQUS / Explicit Ver. 6.8 is employed for numerical simulation. After the above constitutive equation is implemented into a user subroutine, VUMAT, which is one of the customized features of ABAQUS / Explicit, the numerical simulation is performed. Figure 11 shows the computational model that has the same size and shape as the cylindrical specimen used in the experiment. The computational region is discretized using a six-node axisymmetric triangular element with a reduced integration. Under the computational conditions, the vertical displacement of nodes on the bottom is fixed and the shear-free condition is applied. The environmental temperature is set to 296 K. The displacement rate on the upper end is the same as that in the experiment. The crosshead speed of the testing machine in the cases of low strain rate and the time series of strain signals measured from the stress bars of the split Hopkinson pressure bar apparatus for the case of impact testing are given. The displacement rate for the impact test can be calculated using (Yokoyama and Shimizu, 1998)

$$\dot{\delta}(t) = c_0 \{ \varepsilon_i(t) - \varepsilon_r(t) - \varepsilon_i(t) \}. \quad (52)$$

Table 1 shows the identified material parameters for (a) SW1838 and (b) DP-460. Parameters  $s_{\alpha 0}$ ,  $A_{\alpha}$ ,  $\dot{\gamma}_{\alpha 0}^p$ ,  $s_{\beta 0}$ ,  $A_{\beta}$ ,  $\dot{\gamma}_{\beta 0}^p$  and  $s_{\beta 1}$  are identified using Eq. (17) and Fig. 9. Other material parameters are determined by referring to other research works (Boyce et al., 1988; Arruda and Boyce, 1991; Tomita, 2000; Mulliken and Boyce, 2006). From our experimental observation as described previously, the deformation behavior is dealt with as a uniform. This means that no imperfection is introduced and the mesh independency is confirmed.

Figure 12 shows the true stress - true strain diagram obtained by the compression test and by computation under quasi-static to impact loading for (a) SW1838 and (b) DP-460. Figure 12 (a) shows that the model proposed in this study can successfully express the basic features of the curves, such as the linear elastic, strain softening and strain hardening stages, observed for the solidified bulk material of structural adhesives. Almost quantitative correspondence can be observed, and the validity of the proposed model is confirmed. The computational and experimental results also show good agreement in Fig. 12 (b), similarly to Fig. 12 (a). Thus, our model can be widely

applied to structural epoxy adhesive, and the capability of this model can be confirmed.

## 6. CONCLUDING REMARKS

In this study, a bulk specimen made of two types of epoxy resin structural adhesives employed frequently in a mechanical structure was manufactured after solidification. Using the specimen, a compressive test was carried out using an INSTRON-type material testing machine and a split Hopkinson pressure bar method to investigate the stress - strain curve in a wide range of strain rate. As a result, a nonlinear relationship between the yield stress and strain rate was shown. Since it was assumed that the yield stress at a high strain rate is dominated by a secondary relaxation and the mechanism behind secondary relaxation is the presence of rotational degrees of freedom, on the basis of Jones' explanation (Jones, 1985), the plastic shear strain rate in the secondary relaxation was formulated on the basis of an expansion of Argon's formalism (Argon, 1973) using an idea of Li and Gilman (1970). In addition, total shear stress was expressed on the basis of the parallel two-elements model, as was done by Ree and Eyring (1955), using the proposed model and the generalized model of Argon's formula (Argon, 1973).

Taking into account the amorphous glassy polymer after solidification of the adhesive, a rate form of the three-dimensional constitutive equation was formulated on the basis of the four-elements model including an elastic series element, as follows. First, the plastic deformation rate tensor for each relaxation process was formulated by using the effective stress, which represents the difference between total stress, back stress and the stress at each relaxation process, and the formulated plastic shear strain rate. Under the assumption that the plastic deformation rate tensors in the two relaxation processes are the same, a nonlinear simultaneous equation for the stress tensor in each relaxation process was obtained. Including a generalized Hooke's law, a rate form of the three-dimensional constitutive equation can be derived. The proposed constitutive equation was implemented into the commercial finite element code ABAQUS / Explicit and then a finite element simulation was performed. Finally, the validity of the formulated model was shown by comparison with the experimental result.

Two points should be described for unsolved problems. First, the instability can be captured in the stress-strain curve; however, the clear change on the surface cannot be observed like a neck propagation for the tension.

It is valuable to explain this paradox. Second, the fracture can be evaluated by a tension basically. Therefore, tensile behavior of adhesive should be clarified. These points will be discussed in near future.

### **Acknowledgements**

We wish to thank Professor Chiaki SATO of Tokyo Institute of Technology, for providing his valuable guidance on the preparation of the bulk specimen. We also gratefully acknowledged Messer Hideaki KURAMOTO and Norio UESUGI of Hiroshima Municipal Industrial Technology Center, Hiroshima City Industrial Promotion Center, to their assistances on the quasi-static test by their own INSTRON-type material testing machine. The ABAQUS program was provided under academic license by Dassault Systèmes Simulia Corp., Providence, RI.

### **REFERENCES**

- Argon, A. S., 1973. A theory for the low-temperature plastic deformation of glassy polymers. *Philosophical Magazine* 28 (4), 839-865.
- Arruda, E. M., Boyce, M. C., 1991. A three-dimensional constitutive model for the large stretch behavior of rubber elastic materials. *Journal of the Mechanics and Physics of Solids* 41 (2), 389-412.
- Bauwens, J. C., 1972. Relation between the compression yield stress and the mechanical loss peak of bisphenol-A-polycarbonate in the  $\beta$  transition range. *Journal of Materials Science* 7, 577-584.
- Boyce, M. C., Parks, D. M., Argon, A. S., 1988. Inelastic deformation of glassy polymers. Part I: Rate dependent constitutive model. *Mechanics of Materials* 7 (1), 15-33.
- Fay, P. A., 2005. History of adhesive bonding In: Adams, R. D. (Eds.), *Adhesive Bonding - Science, technology and applications* -. Woodhead Publishing Ltd., pp. 2-18.

- Goglio, L., Peroni, L., Peroni, M., Rossetto, M., 2008. High strain-rate compression and tension behavior of an epoxy bi-component adhesive. *International Journal of Adhesion and Adhesives* 28 (7), 329-339.
- Haward, R. N., Thackray, G., 1968. The use of a mathematical model to describe isothermal stress-strain curves in glassy thermoplastics. *Proceedings of the Royal Society of London A302 (1471)*, 453-472.
- Hutchinson, J. M., 1973. Relaxation processes and physical aging. In: Haward, R. N., Young, R. J. (Eds.), *The physics of glassy polymers*. Chapman & Hall, pp. 128-129.
- Jones, A. A., 1985. Molecular level model for motion and relaxation in glassy polycarbonate. *Macromolecules* 18 (5), 902-906.
- Kolsky, H., 1949. An investigation of the mechanical properties of materials at very high rates of loading. *Proceedings of the Physical Society B62 (2)*, 676-700.
- Li, J. C. M., Gilman, J. J., 1970. Disclination loops in polymers. *Journal of Applied Physics* 41 (11), 4248-4256.
- Mulliken, A. D., Boyce, M. C., 2006. Mechanics of the rate-dependent elastic-plastic deformation of glassy polymers from low to high strain rates. *International Journal of Solids and Structures* 43 (5), 1331-1356.
- Nakai, K., Yokoyama, T., 2008. Strain rate dependence of compressive stress-strain loops of several polymers. *Journal of Solid Mechanics and Materials Engineering* 2 (4), 557-566.
- Nemat-Nasser, S., Issacs, J. B., Starrett, J. E., 1991. Hopkinson bar techniques for dynamic recovery experiments. *Proceedings of the Royal Society of London A435 (1894)*, 371-391.
- Nishida, M., Ito, N., Tanaka, K., 2009. Effects of strain-rate and temperature on compressive properties of oil-based biodegradable plastics. *Zairyo* 58 (5), 414-420. (in Japanese)
- Ree, T., Eyring, H., 1955. Theory of non-newtonian flow. I. Solid plastic system. *Journal of Applied Physics* 26 (7), 793-800.
- Sato, C., Ikegami, K., 1999. Strength of adhesively-bonded butt joints of tubes subjected to combined high-rate loads. *Journal of Adhesion* 7 (1 & 2), 57-73.

- Sato, C., Ikegami, K., 2001. Dynamic deformation of lap joints and scarf joints under impact loads. *International Journal of Adhesion and Adhesives* 20 (1), 17-25.
- Tomita, Y., 2000. Constitutive modelling of deformation behavior of glassy polymers and applications. *International Journal of Mechanical Sciences* 42 (8), 1455-1469.
- Yokoyama, T., Shimizu, H., 1998. Evaluation of impact shear strength of adhesive joints with the split Hopkinson bar. *JSME International Journal Series A* 41 (4), 503-509.
- Yu, X. X., Crocombe, A. D., Richardson, G., 2001. Material modelling for rate-dependent adhesives. *International Journal of Adhesion and Adhesives* 21 (3), 197-210.

## FIGURE CAPTIONS

Figure 1. Measurement result of differential scanning calorimetry against environmental temperature for the structural adhesives (a) SW1838 and (b) DP - 460

Figure 2. Schematic illustration of the split Hopkinson bar apparatus used here

Figure 3. Output signals from the strain gauges glued on the input and output stress bars (a) without pulse shaper and (b) with pulse shaper.

Figure 4. Time history of compressive force of adhesive bulk material during impact compressive test (a) without and (b) with pulse shaper

Figure 5. True stress-true strain curves of structural adhesives (a) SW1838 and (b) DP - 460 obtained by quasi-static to impact compressive tests

Figure 6. Yield behavior in uniaxial compression as a function of strain rate for structural adhesives SW1838 and DP - 460

Figure 7. Schematic illustrations of folded molecular chain with an angle of kink  $\omega$  and a chain length of segment  $z$  given by Argon (1973).

Figure 8. Schematic illustrations of folded molecular chain with an angle of kink  $\omega$  and twist rotation  $\theta$

Figure 9. Comparison of a compressive yield stress - strain rate relationship obtained by the experiment and the formulated model

Figure 10. Four elements elasto-viscoplastic model including each relaxation process

Figure 11. Finite element model for compressive specimen

Figure 12. Comparison of stress - strain curve for the structural adhesive (a) SW1838 and (b) DP - 460 obtained by the experiment and the computation

## TABLE CAPTIONS

Table 1. Material parameters for (a) SW1838 and (b) DP-460.

## TABLES

Table 1. Material parameters for (a) SW1838 and (b) DP-460.

(a)			(b)		
$E$ [GPa]	$\nu$	$T$ [K]	$E$ [GPa]	$\nu$	$T$ [K]
1.8	0.3	296	1.1	0.3	296
$s_{\alpha 0}$ [MPa]	$A_{\alpha}$ [K·MPa <sup>-1</sup> ]	$\dot{\gamma}_{\alpha 0}$ [s <sup>-1</sup> ]	$s_{\alpha 0}$ [MPa]	$A_{\alpha}$ [K·MPa <sup>-1</sup> ]	$\dot{\gamma}_{\alpha 0}$ [s <sup>-1</sup> ]
76.2	190.9	$1.1 \times 10^8$	46.2	274.5	321.8
$s_{\beta 0}$ [MPa]	$A_{\beta}$ [K·MPa <sup>-1</sup> ]	$\dot{\gamma}_{\beta 0}$ [s <sup>-1</sup> ]	$s_{\beta 0}$ [MPa]	$A_{\beta}$ [K·MPa <sup>-1</sup> ]	$\dot{\gamma}_{\beta 0}$ [s <sup>-1</sup> ]
1.82	19.9	798.2	3.55	43.1	226.6
$s_{\beta 1}$ [MPa]	$C_R$ [MPa]	$\sqrt{N}$	$s_{\beta 1}$ [MPa]	$C_R$ [MPa]	$\sqrt{N}$
0.18	12.7	1.47	0.09	12.7	1.47
$h_{\alpha}$	$h_{\beta}$	$s_{ss,\alpha}$ [MPa]	$h_{\alpha}$	$h_{\beta}$	$s_{ss,\alpha}$ [MPa]
250	250	79.3	90	90	57.4
$s_{ss,\beta}$ [MPa]	$\alpha_{\alpha}$ [MPa]	$\alpha_{\beta}$ [MPa]	$s_{ss,\beta}$ [MPa]	$\alpha_{\alpha}$ [MPa]	$\alpha_{\beta}$ [MPa]
79.3	0.08	0.08	57.4	0.08	0.08

## FIGURES

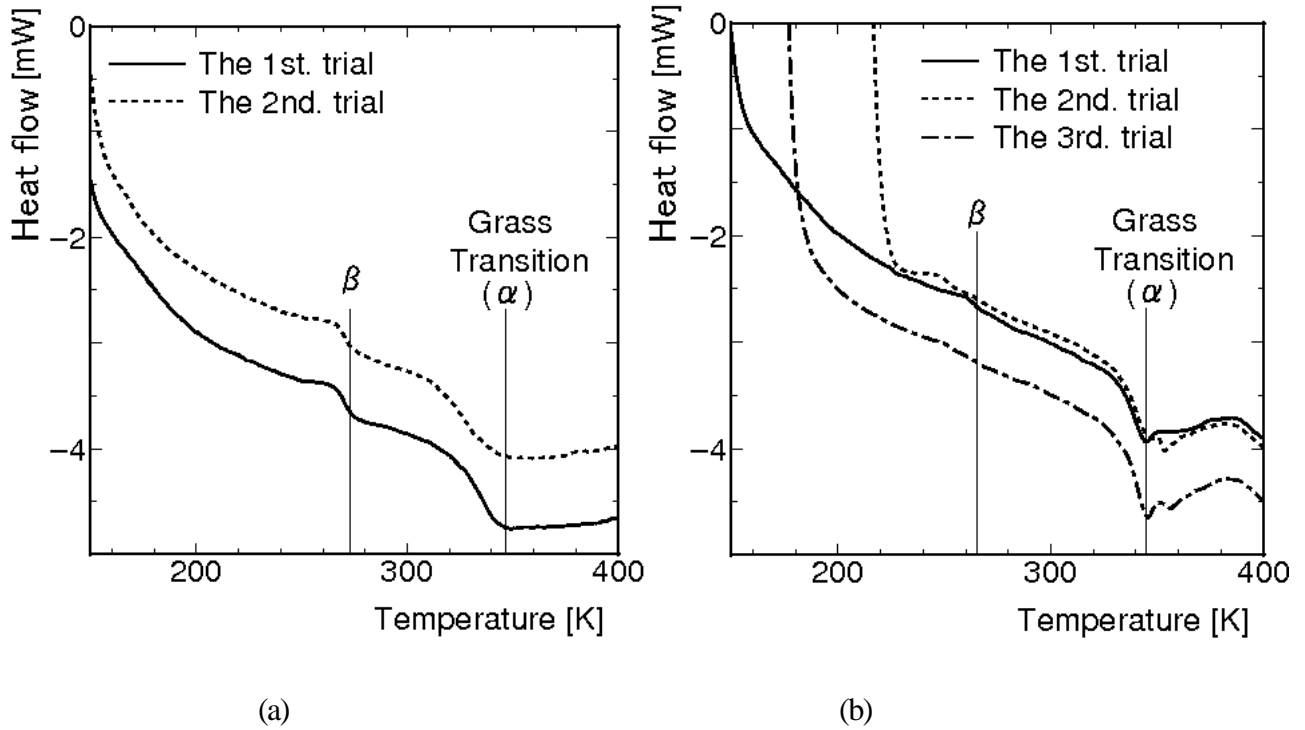


Figure 1. Measurement result of differential scanning calorimetry against environmental temperature for the structural adhesives (a) SW1838 and (b) DP - 460.

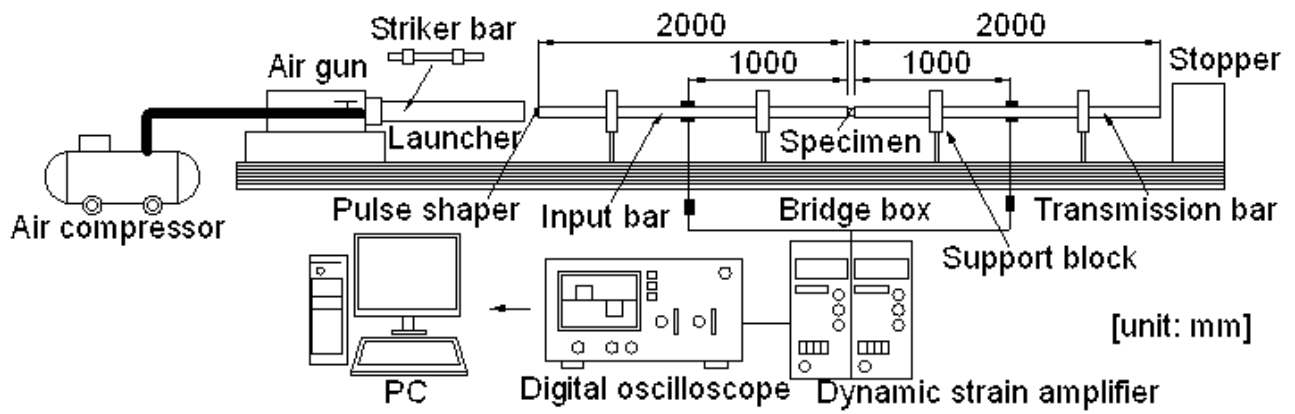
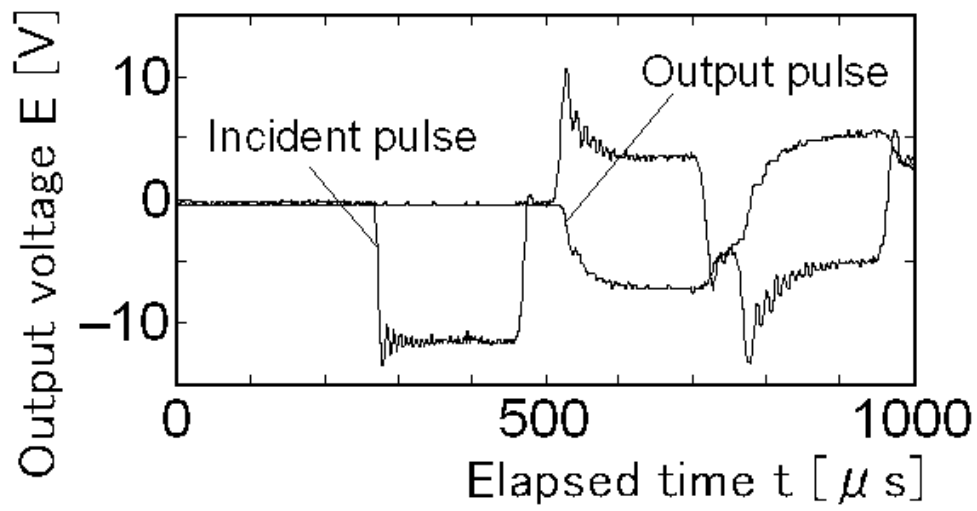
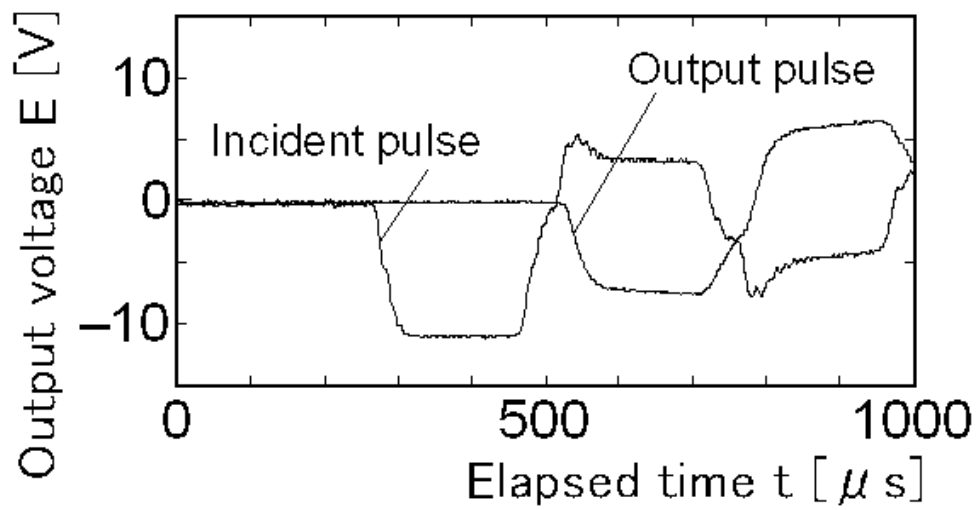


Figure 2. Schematic illustration of the split Hopkinson bar apparatus used here.

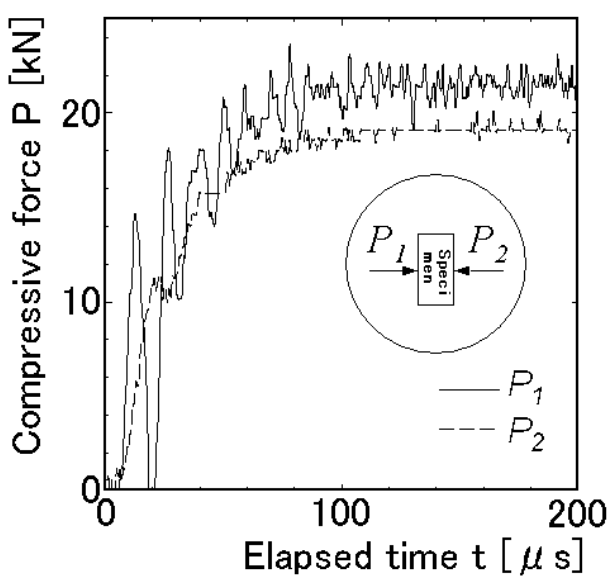


(a)

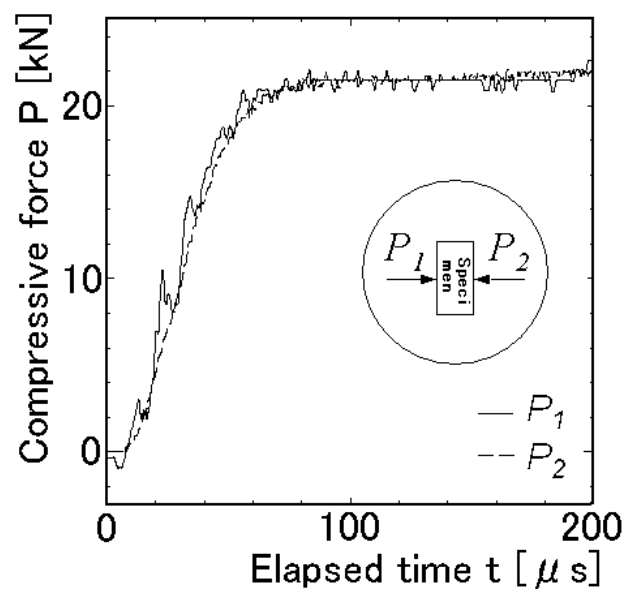


(b)

Figure 3. Output signals from the strain gauges glued on the input and output stress bars (a) without pulse shaper and (b) with pulse shaper.

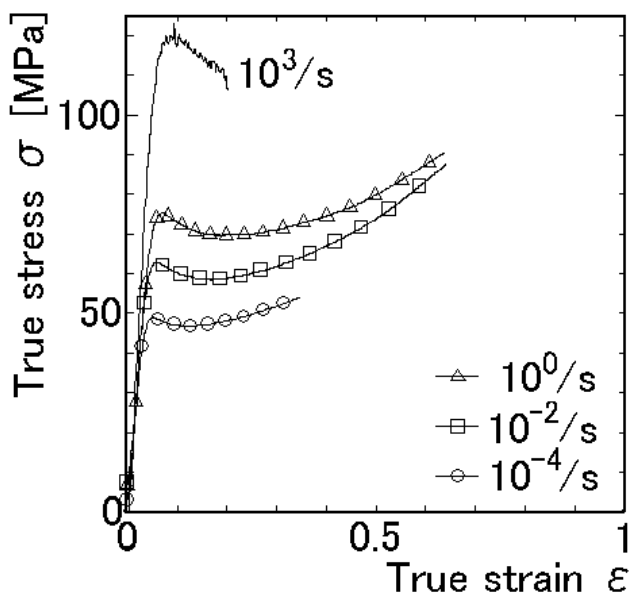


(a)

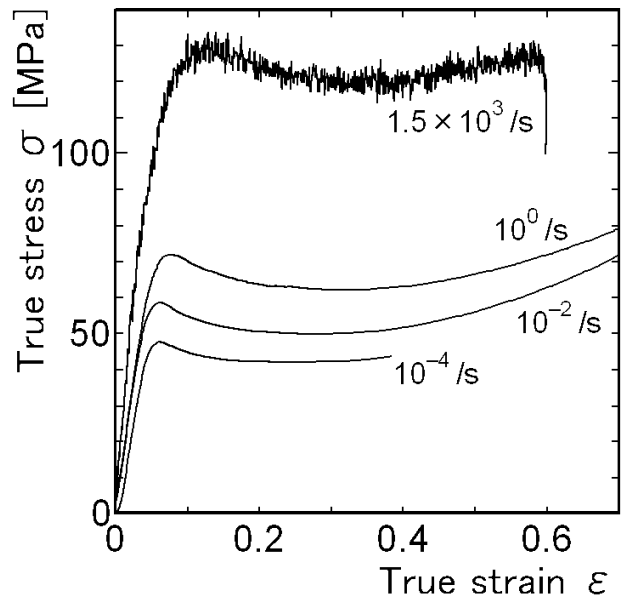


(b)

Figure 4. Time history of compressive force of adhesive bulk material during impact compressive test (a) without and (b) with pulse shaper.



(a)



(b)

Figure 5. True stress-true strain curves of structural adhesives (a) SW1838 and (b) DP - 460 obtained by quasi-static to impact compressive tests.

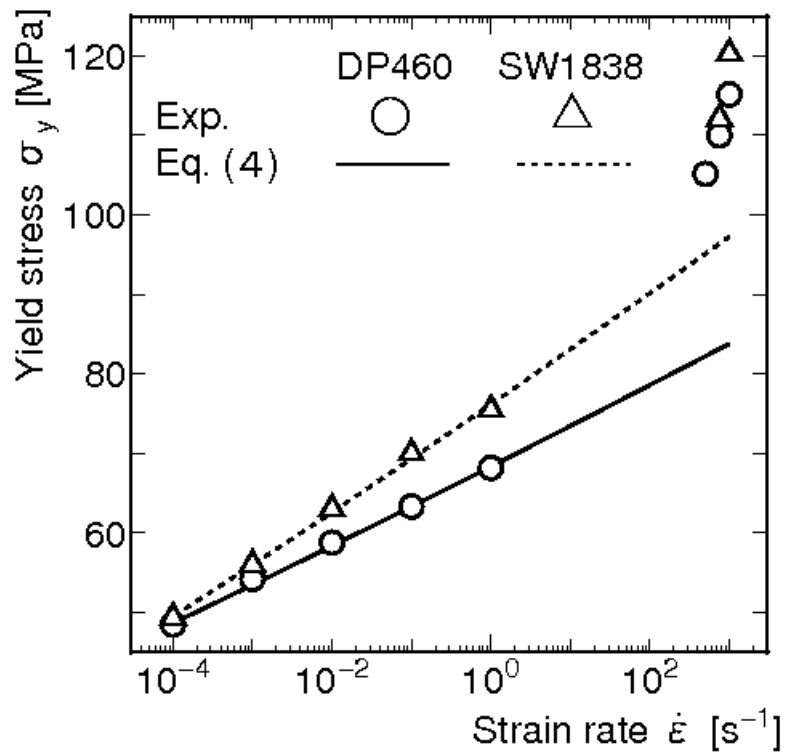


Figure 6. Yield behavior in uniaxial compression as a function of strain rate for structural adhesives SW1838 and DP -

460.

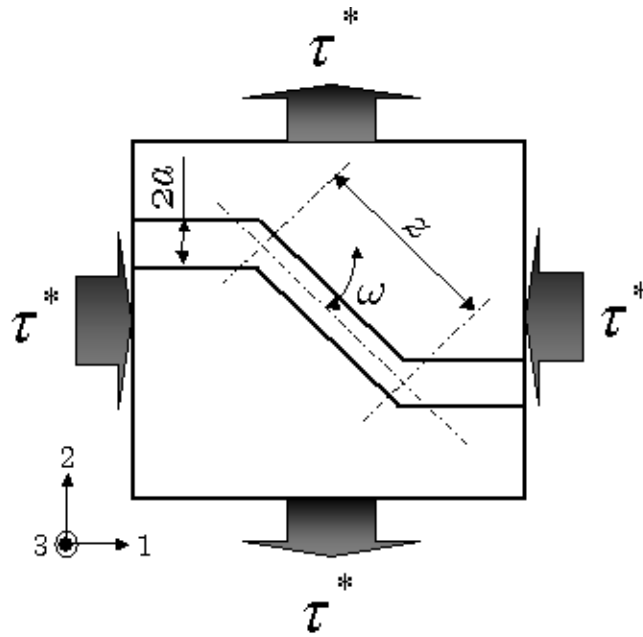


Figure 7. Schematic illustrations of folded molecular chain with an angle of kink  $\omega$  and a chain length of segment  $z$  given by Argon (1973).

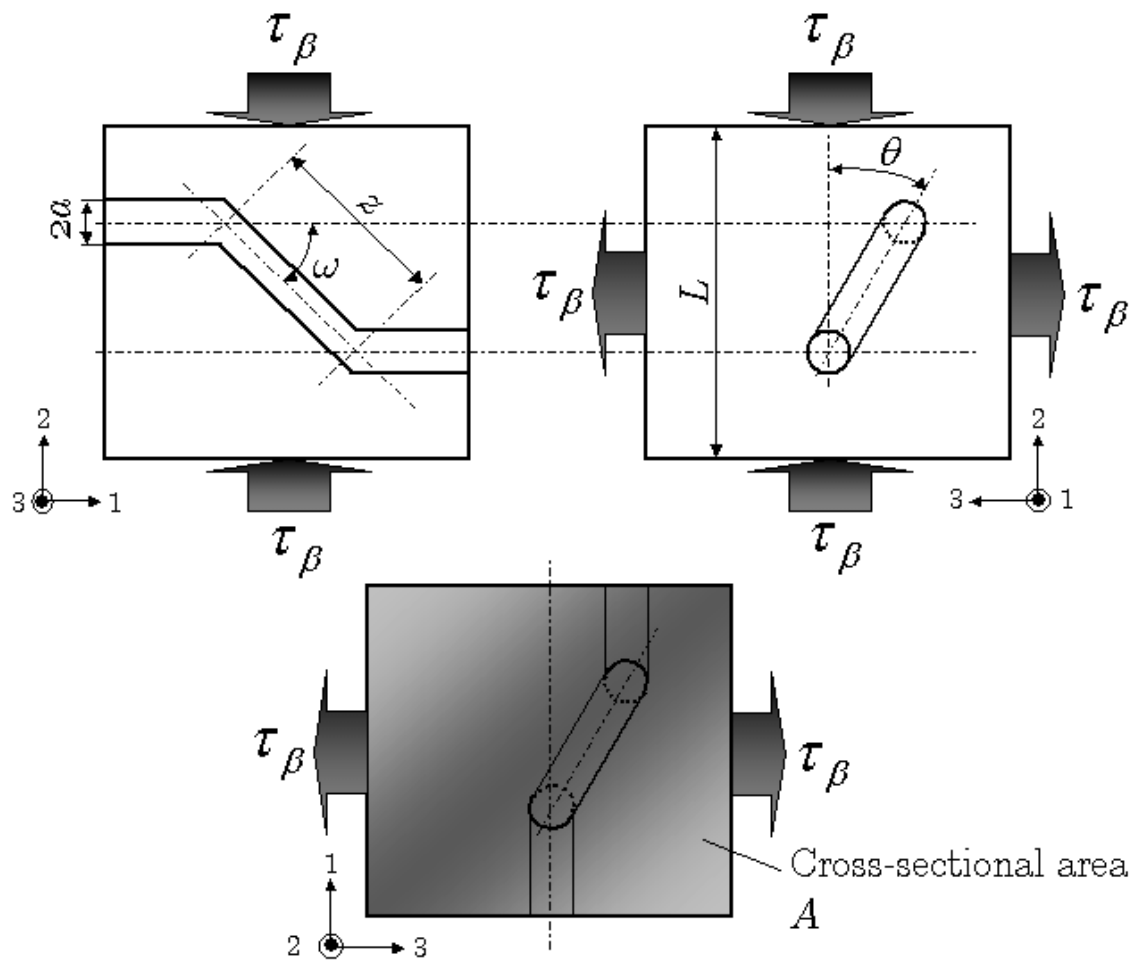


Figure 8. Schematic illustrations of folded molecular chain with an angle of kink  $\omega$  and twist rotation  $\theta$ .

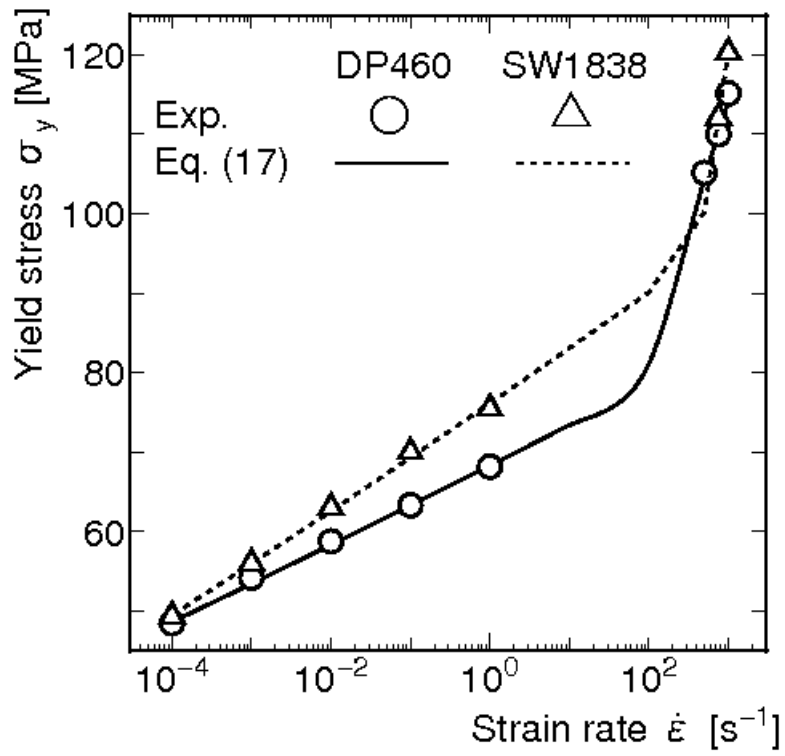


Figure 9. Comparison of a compressive yield - strain rate relationship obtained by the experiment and the formulated model.

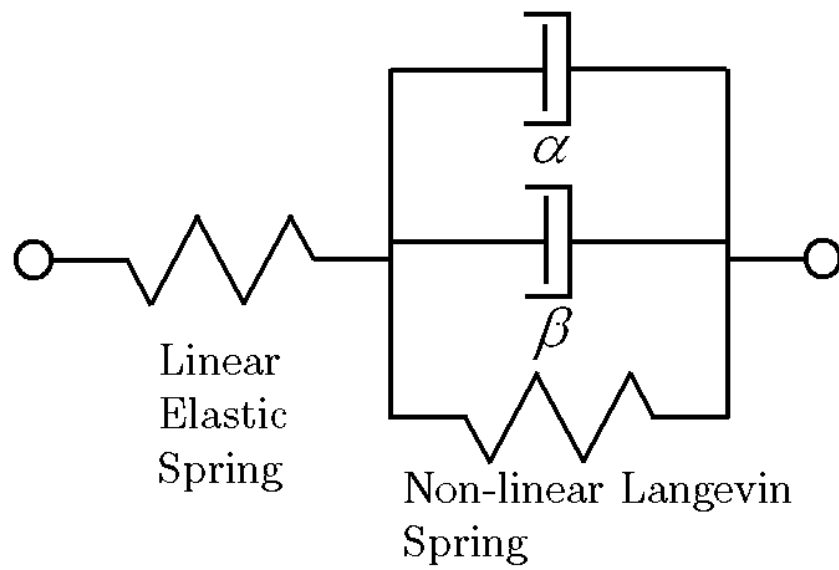


Figure 10. Four elements elasto-viscoplastic model including each relaxation process.

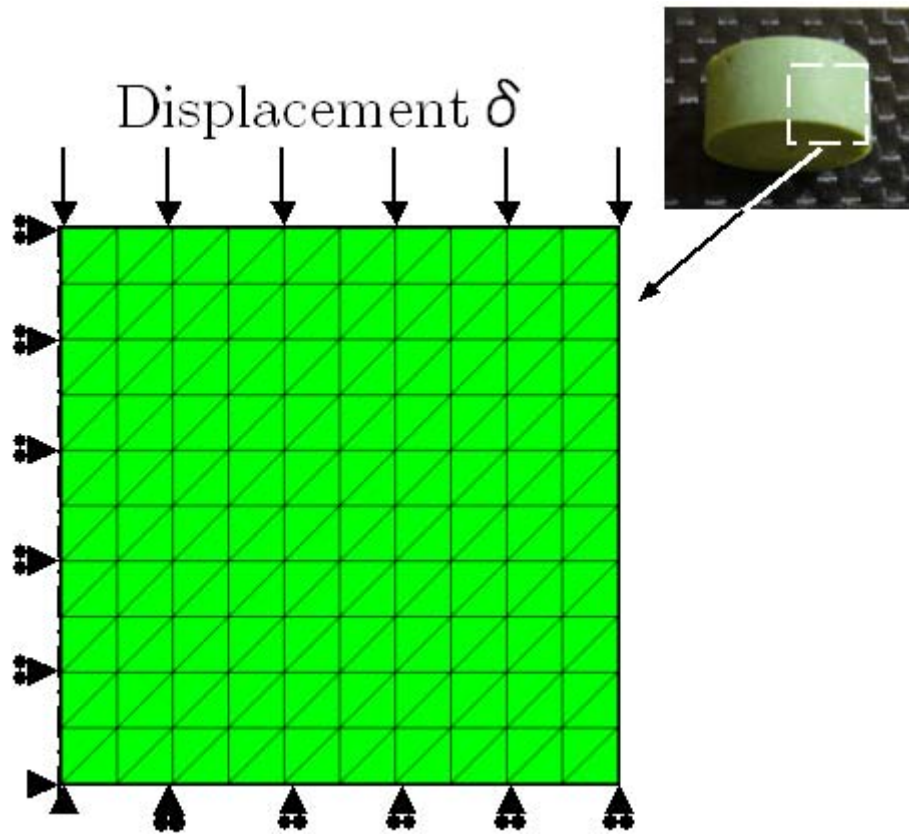


Figure 11. Finite element model for compressive specimen.

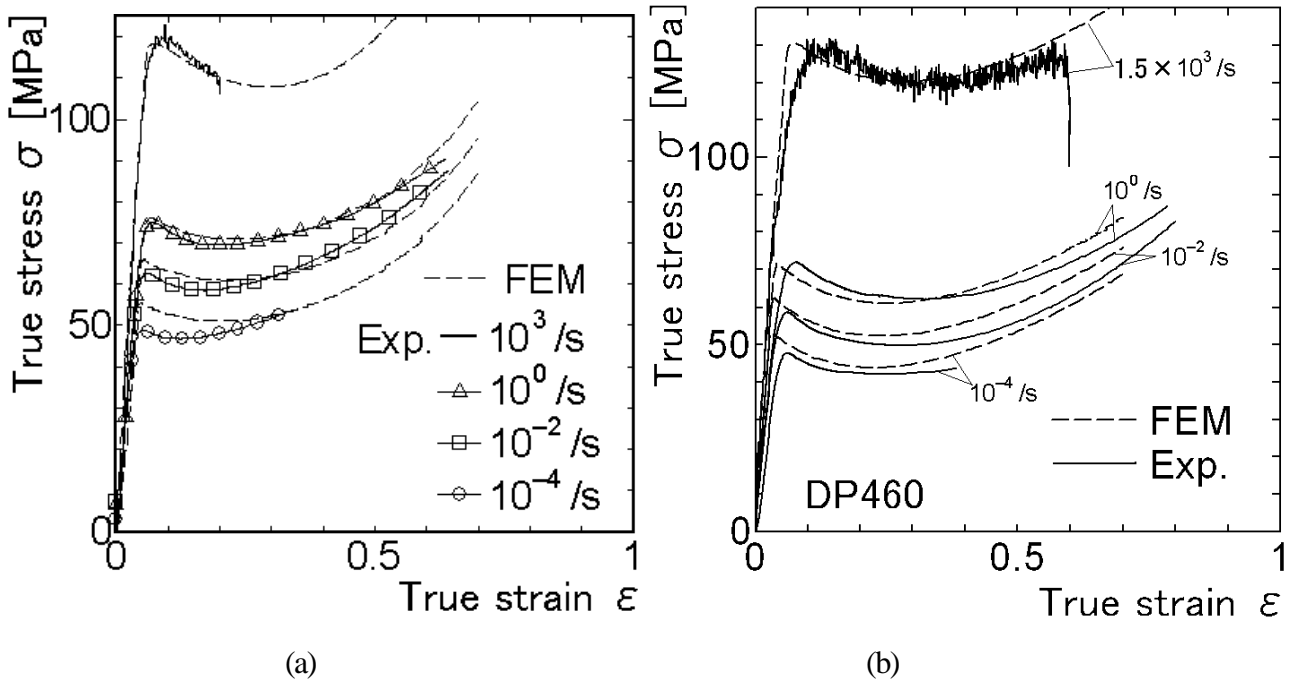


Figure 12. Comparison of stress - strain curve for the structural adhesive (a) SW1838 and (b) DP - 460 obtained by the experiment and the computation